JOURNAL OF SPACECRAFT AND ROCKETS
Vol. 45, No. 4, July–August 2008

Transient Modeling of High-Altitude Rocket-Stage Separation

Allen Eramya*
University of Southern California, Los Angeles, California 90089
Jason Cline† and Matthew Braunstein‡
Spectral Sciences Inc., Burlington, Massachusetts 01803
and
Sergey Gimelshein§
University of Southern California, Los Angeles, California 90089

DOI: 10.2514/1.34784

The direct simulation Monte Carlo method is used to model a transient stage separation of a generic sounding rocket at 100 km. Lower-stage movement is included, and the flow and surface properties are simulated during the first second after thruster ignition. Both liquid and solid propellant thrusters are examined with a thrust of 25 and 34 kN, respectively. Four different simulation scenarios are considered that allow analysis of the impact of the stage motion, explicitly including unsteady flow effects. Unsteady flow effects are small enough that quasi-steady-state modeling appears to be adequate for this general staging scenario. The influence of direct simulation Monte Carlo statistical fluctuations on the stage trajectory is insignificant compared with the total contribution of the plume force. We also examine the radiation environment, including the plume–atmosphere shock and plume–lower-stage impingement.

Nomenclature

$\hat{\mathbf{e}}_s$	=	rocket direction before separation
$\mathbf{F}_d$	=	atmospheric drag force, N
$\mathbf{F}_p$	=	force of the lower stage due to plume impingement, N
$\mathbf{g}$	=	gravitational acceleration, m/s^2
m	=	stage mass, kg
N	=	number of time steps between stage movements
$\mathbf{T}$	=	rocket thrust force, N
t	=	time after separation, s
$\mathbf{v}$	=	stage velocity, m/s
$\mathbf{v}_s$	=	initial individual stage velocity, m/s
$\mathbf{v}_{\text{sep}}$	=	initial stage-separation velocity, m/s
$\Delta\mathbf{v}$	=	stage-separation velocity, m/s

Subscripts

x, y	=	axial and radial directions, respectively
1, 2	=	lower and upper stages, respectively

I. Introduction

OVER the last two decades, the direct simulation Monte Carlo (DSMC) method has gradually evolved into a powerful and versatile technique. The DSMC method has been successfully applied to many complex problems of modern rarefied gas dynamics, primarily related to high-altitude aerodynamics and microscale flows [1]. However, nearly all current applications of the DSMC method deal with gas flows interacting with stationary or pseudostationary gas–surface interfaces. Two exceptions are the work of Oran et al. [2], who modeled a rotating ellipse using a monotonic Lagrangian grid technique, and the work of Gallis and Torczinki [3], who examined flow over moving microbeams using both continuum (Navier–Stokes) and kinetic (DSMC) approaches. There is therefore a large gap between the relatively mature state of continuum modeling of moving solid interfaces (such as fixed-wing aircraft, rotor aircraft, and turbomachinery applications) and particle-based approaches such as DSMC, in which capabilities such as six-degree-of-freedom (6-DOF) body motions and conjugate heat transfer are in relatively early stages. There are several major challenges that limit current applications of the DSMC method to study gas flows with moving solid boundaries. These include algorithmic, mostly grid-related difficulties of efficient realization of the DSMC method, especially for a free-body motion with arbitrary shape changes, and numerical problems that arise due to the subsonic nature of these flows.

To help extend the DSMC method as a practical tool for rarefied time-dependent flows, we present results for a generic high-altitude (~100 km) sounding-rocket-stage-separation scenario in which the relative atmosphere-rocket speed is 5 km/s. We examine two cases: a liquid propellant with 25-kN thrust and a solid propellant with 34-kN thrust. In our calculations, the upper-stage thruster fires on a lower stage (0.75-m-diam, 3-m-long cylinder) that is initially at a 2-m separation with an initial relative velocity of 2 m/s. These parameters, along with a high thruster-related acceleration, represent typical conditions for a very fast stage separation and are used to emphasize the transience of the process. Figure 1 shows the basic stage-separation scenario.

The primary goals of this study are to determine the practicality of using DSMC for stage separation in a rarefied atmosphere and to compare quasi-steady-state treatments with fully time-dependent results. The initial stage-separation velocities and other parameters in the flow are therefore chosen to stress steady-state assumptions, but at the same time, the parameters reflect practical scenarios. Another important element in the present study is the determination of forces and heat loads on the lower stage, as well as determination of the radiation signature due to interaction of the upper-stage plume with the atmosphere and impingement of the upper-stage plume on the lower stage. We have therefore performed a matrix of calculations with the preceding generic stage-separation scenario that includes: 1) steady state with lower stage, 2) unsteady with moving lower stage, 3) unsteady with a fixed lower stage, and 4) unsteady with no lower stage.

One of the main results we found is that numerical convergence can be practically achieved within our DSMC approach for our

Presented as Paper 4410 at the 39th AIAA Thermophysics Conference, Miami, FL, 25–28 June 2007; received 25 September 2007; revision received 20 December 2007; accepted for publication 3 January 2008.

*Research Assistant.
†Principal Scientist.
‡Group Leader, Computational Physics and Chemistry.
§Research Assistant Professor, Department of Aerospace and Mechanical Engineering.

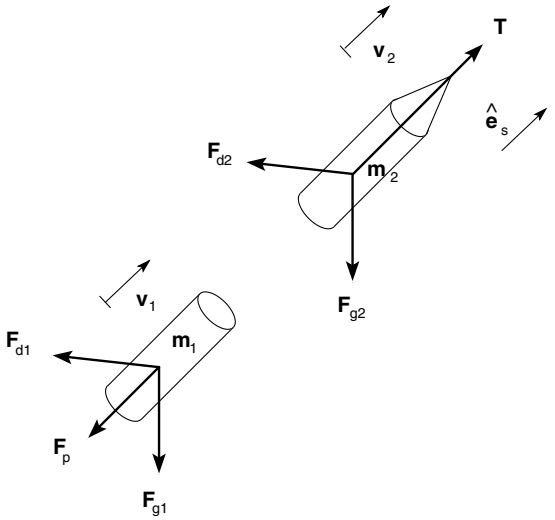

Fig. 1 Free-body diagram of the two-stage system after separation. Subscript 2 denotes the upper stage, and subscript 1 denotes the lower stage.

unsteady and steady calculations. Another significant finding is that the steady-state runs with the lower stage at a fixed distance (quasi steady) closely match the full unsteady results. Because the scenario conditions are at the upper end of practical applications in terms of velocities and thrusts and would be most likely to show unsteady effects if they were present, our results show that quasi-steady-state calculations are adequate to describe most rarefied stage-separation scenarios. This makes examination of such phenomena much more practical with DSMC. The major features of the flow are a plume–atmosphere shock/mixing layer, the plume–gas impingement shock on the lower stage, and the particle flow and impingement on the lower stage. The plume–atmosphere shock, which reaches 10,000 K in translational temperature, appears to be completely independent of the presence of the lower stage for the conditions examined. We also generated radiation maps of our flowfields for a sensor viewing the flow from a large distance. We note that the stage-separation problem has been treated before in the context of continuum fluid dynamics [4]. To our knowledge, however, the present work is the first application of DSMC to time-dependent stage separation in a rarefied atmosphere.

II. Stage-Separation Forces

Before discussing the particulars of the numerical approach, it is useful to define the forces and other dynamic variables that play a role in the stage-separation scenario being considered. Before stage separation, the rocket is oriented in the $\hat{\mathbf{e}}_s$ direction. The lower stage turns off, causing the vehicle to enter free fall under gravitational acceleration g. At this point, both stages are attached to each other. Then a separation mechanism provides an impulse of force, causing the upper and lower stages to separate from each other with initial relative velocity $\mathbf{v}_{\text{sep}}$, where the individual stages' velocities are $\mathbf{v}_{2,s} - \mathbf{v}_{1,s} = \mathbf{v}_{\text{sep}}$. The separated stages are in free fall for time duration t_s, after which the upper-stage propulsion fires.

Figure 1 shows the free-body diagram for the system. The gas flow exerts force on the bodies through thrust $\mathbf{T}$, plume impingement $\mathbf{F}_p$, and drag $\mathbf{F}_{d1}$ and $\mathbf{F}_{d2}$. Gravity, of course, exerts a force proportional to object mass: $\mathbf{F}_{gi} = m_i\mathbf{g}$. If we then define $t = 0$ as the time immediately after separation, the stage velocities can be related to the forces

$$\begin{aligned}\mathbf{v}_1(t) &= \mathbf{v}_{1,s} + \int_0^t \frac{\mathbf{F}_{g1} + \mathbf{F}_p + \mathbf{F}_{d1}}{m_1}\,\mathrm{d}t \\ &= \mathbf{v}_{1,s} + \int_0^t \mathbf{g} + \frac{\mathbf{F}_p}{m_1} + \frac{\mathbf{F}_{d1}}{m_1}\,\mathrm{d}t\end{aligned} \tag{1}$$

$$\begin{aligned}\mathbf{v}_2(t) &= \mathbf{v}_{2,s} + \int_0^t \frac{\mathbf{F}_{g2} + \mathbf{T} + \mathbf{F}_{d2}}{m_2}\,\mathrm{d}t \\ &= \mathbf{v}_{2,s} + \int_0^t \mathbf{g} + \frac{\mathbf{T}}{m_2} + \frac{\mathbf{F}_{d2}}{m_2}\,\mathrm{d}t\end{aligned} \tag{2}$$

We assume that the distance between stages is not so large as to produce a discernible change in the gravity $\mathbf{g}$ vector. We further constrain $\mathbf{v}_{1,2}(t = 0)$ and $\mathbf{v}_{\text{sep}}$ to be parallel to $\hat{\mathbf{e}}_s$, so that there is no angle of attack. (The apparent direction of the drag force vector in Fig. 1 is a generalization.) The resulting separation velocity is then independent of gravity:

$$\Delta\mathbf{v}(t) = \mathbf{v}_2(t) - \mathbf{v}_1(t) = \mathbf{v}_{\text{sep}} + \int_0^t \frac{\mathbf{T} + \mathbf{F}_{d2}}{m_2} - \frac{\mathbf{F}_p + \mathbf{F}_{d1}}{m_1}\,\mathrm{d}t \tag{3}$$

In this simple linearly translating system, we may use a gravitationally accelerated reference frame. Gravity's main effect would be to change the velocity of the atmosphere relative to the vehicles, but for short time durations (1 s) the error is less then 10 m/s, which is negligible compared with the original velocity of 5000 m/s.

Because we are at 100-km altitude and the time under consideration is relatively short (1 s), the atmospheric drag forces are small compared with the thrust and plume-induced forces, further reducing the time-dependent separation relation:

$$\Delta\mathbf{v}(t) \approx \mathbf{v}_{\text{sep}} + \int_0^t \frac{\mathbf{T}}{m_2} - \frac{\mathbf{F}_p}{m_1}\,\mathrm{d}t \tag{4}$$

Important to this assumption is the orientation of the vehicle axis parallel to the direction of travel. Although the drag force is small compared with the thrust and plume impingement forces, the system is more sensitive to lateral (i.e., $\perp \hat{\mathbf{e}}_s$) perturbations in alignment of the stages, because they could cause the lower stage to tumble.

III. Numerical Approach

The DSMC method is used to model the stage separation with the lower stage moving away from the upper stage, and a number of changes need to be introduced into the standard DSMC algorithm to account for this motion. The DSMC method is a statistical approach to the solution of the Boltzmann equation. The gas system is modeled by a finite number of simulated particles, with their mean free paths corresponding to those of real gas molecules. A DSMC solution tends to the solution of the Boltzmann equation when the number of simulated particles tend to infinity (no statistical correlations between them). The conventional DSMC algorithm includes spatial and temporal discretization, with the division of the computational domain into collision cells and of continuous time into finite time steps.

The principal changes in the DSMC algorithm incorporated in this work include 1) stage motion under the impact of the two main contributing forces, $\mathbf{T}$ and $\mathbf{F}_p$, 2) collisions of molecules with the moving stage, and 3) displacement of molecules by the moving stage. To incorporate these changes, the following algorithms are used.

A. Stage Motion

The lower stage will move every N time steps ($N = 100$ was used in this work), with the condition that the stage displacement is small compared with the distance between the stages and lower-stage size. This condition will ensure that the impact of discretization of the stage motion on the flowfield is small. The distance that the stage is displaced is proportional to $N\Delta t$ and the relative stage velocity $\Delta\mathbf{v}$ described in the previous section. Here, Δt is the time step, and the velocity $\Delta\mathbf{v}$ depends on the value of the plume force $\mathbf{F}_p$ and the constant thrust force $\mathbf{T}$. Note that for simplicity, a noninertial frame of reference that is fixed to the upper stage is used, and the acceleration of gas molecules due to the stages' acceleration in an inertial reference frame is not accounted for. This effect is believed to be small, because the total molecular velocity change relative to the

stages over the period of time under consideration will not exceed 3%.

Because the plume force $\mathbf{F}_p$ changes as the stage separation increases, the current value of $\mathbf{F}_p$ is used to estimate the plume-force-related contribution to $\Delta\mathbf{v}$. The current value was obtained through the averaging of the surface properties using gas–surface collisions that occur over the last M time steps before the actual stage motion ($M = 10$ was used in this work). In the axisymmetric simulations presented in this paper, only the drag component of the plume force is accounted for, and the lower stage moves only along the plume axis. In the two-dimensional simulations, both lift and pitching moment are included, and the stage is allowed to move off the plume axis and to rotate. This kind of motion could occur due to DSMC statistical errors, which may create asymmetric forces. Therefore, such tests are a measure of the robustness of our DSMC moving-body algorithms. For the rotation, the center of mass was assumed to be the geometric center of the lower stage. In the algorithms presented in this paper, the stage rotation is not accounted for, and only translational motion is assumed to be contributing to gas–surface collisions and molecule displacement.

B. Gas–Surface Collisions

Because the stage motion is modeled in the reference frame of the upper stage, gas–surface collisions with the upper stage are modeled as usual. For the gas–surface collisions with the lower stage, molecular velocities after collision (normal and tangential components) are sampled according to the conventional fully diffuse reflection, which reflects the assumed lower-stage temperature, plus the added velocity that corresponds to the translational velocity of the body.

C. Molecule Displacement

To displace molecules by the moving stage, after each N time steps, the following simple algorithm is used, which conserves mass and energy:

1) For each molecule in the computational domain, check if it is close enough to the lower stage's center of mass (this excludes from consideration a number of molecules far from the surface).

2) If a molecule is close to the center of mass, compute its collision time with the stage t_c, assuming the stage does not move and the molecule moves with the velocity $(-\Delta\mathbf{v}_x, 0, 0)$ in the axisymmetric case and $(-\Delta\mathbf{v}_x, -\Delta\mathbf{v}_y, 0)$ in the 2D Cartesian case. Here, $(\Delta\mathbf{v}_x, \Delta\mathbf{v}_y)$ are the components of the current stage velocity.

3. If $t_c < N\Delta t$, compute new coordinates of the molecule as if it had a velocity $-\Delta\mathbf{v}$ and experienced a specular collision with the surface, as

$$-\Delta\mathbf{v}t_c + \Delta\mathbf{v}(N\Delta t - t_c) + \Delta\mathbf{v}N\Delta t = 2\Delta\mathbf{v}(N\Delta t - t_c)$$

To implement these algorithms, we use the SMILE DSMC code [5] and extend it with the free-cell method [6], which avoids a potentially numerically intensive and complex grid reconstruction step during the stage motion.

IV. Flow Conditions and Parameters of the Approach

We consider a generic sounding rocket that consists of a cone–cylinder upper stage and a cylinder lower stage. The diameter of both stages is assumed to be 0.75 m, the length of the upper and lower stages is 3 m, and the conical part is 1 m long. The upper- and lower-stage masses are 350 and 125 kg, respectively. This results in a thrust-based acceleration of the upper stage of about 70 m/s^2. We use an atmosphere of N_2 at conditions approximating 100-km altitude and perform calculations up to 1 s when the lower stage is 50 m from the upper stage. The staging is calculated at a freestream velocity of 5 km/s, and the atmosphere is assumed to have a temperature of 190 K and number density of 8.5×10^{18} m^{-3}. The stage surface temperature is uniform at 500 K. Initial stage-separation distance and velocity are 2 m and 2 m/s, respectively.

Two types of thrusters are considered: liquid and solid propellant thrusters. In both thrusters, the gas stagnation pressure and temperature are 35 atm and 3000 K, respectively. To simplify flow analysis, the gas plume was presented as a 75% CO and 25% H_2O mixture. The nozzle throat and exit diameters are 7 and 50 cm, respectively, and the diverging part half-angle is 15 deg. The resulting thrust for the liquid propellant thruster is about 25 kN. In the solid propellant thruster, in addition to the component gas, two alumina particle sizes are modeled with diameters of 0.2 and 3.6 μm. The aluminum particle loading is about 20%, and the resulting thrust is about 34 kN.

The flow inside the nozzle is modeled using CFD++ software [7]. CFD++ is a flexible computational fluid dynamics software suite for the solution of steady and unsteady, compressible and incompressible Navier–Stokes equations, including multispecies capability for perfect and reacting gases. In this work, a reacting-gas compressible Navier–Stokes solver is used with second-order spatial discretization and implicit time integration; a general multiphase capability was used that provides an Eulerian description of the disperse phase (particulates). The macroparameter profiles at the nozzle exit are obtained using a single-block rectangular grid with a total of about 20,000 nodes. The inflow and outflow boundary conditions are stagnation pressure and temperature, and back-pressure imposition (the value of 1 Pa is assumed), respectively. A symmetry condition is used at the plume axis. The isothermal boundary with a surface temperature of 1000 K is assumed at the nozzle surface.

The plume expanding into a rarefied atmosphere of 100 km of N_2 is computed using the SMILE computational tool [5] based on the DSMC method. A starting surface at the nozzle exit plane is used to model plume boundary conditions with parameters obtained using CFD++. About 10 million molecules and 300,000 background collision cells were used. The number of sampling cells is about 350,000. A time step of 10^{-5} s was used and the body movement occurred every 100 time steps (0.001 s). The change in stage-separation distance over this time is smaller than 0.1%, which is considered adequate in terms of numerical accuracy. Note that near the nozzle exit, the cell size and the time step do not satisfy the conventional DSMC requirements, and a collision limiter [8] was used there to reduce computational time. To check the accuracy of results, a single calculation was conducted with about four times the number of molecules and two-times-smaller linear cell size and time step. The difference between the results was found to be within statistical scatter. The numerical approximations used in our DSMC implementation therefore should not be a significant source of error.

The variable hard sphere model is used for gas–gas collisions, and a diffuse reflection model is used for gas scattering with surfaces. The gas–particulate interaction is modeled with the approach of Gallis et al. [9] using two-way coupling [10]. The DSMC modeling accounts for the plume impingement forces and lower-stage movement. Lacking experimental guidance at the relative velocities of interest, we assume a diffuse reflectance model for particulate reflection from the lower stage. The lack of a validated or generally accepted particulate–surface interaction model is a significant gap in the modeling of such scenarios. Most calculations used axial symmetry. All axisymmetric computations were conducted using radial weights. Species weights are used to reduce the statistical scatter for the freestream species and particulates.

V. Stage Separation Driven by a Liquid Propellant Thruster

The first set of computations was conducted for a 25-kN liquid propellant thruster, and the stage separation was modeled during the first second after thruster ignition. To understand the role of lower-stage motion on the flow and to examine several key modeling assumptions, the following four cases were considered. First, unsteady full-stage motion is modeled as a result of the thrust force $\mathbf{T}$ propelling the upper stage and the force $\mathbf{F}_p$ from the plume impinging on the lower stage. Second, the flow was computed for an unsteady plume development but a fixed-body geometry (two

geometries were considered for the time after ignition of 0.3 and 1 s). Third, an unsteady plume development was simulated at 0.3 and 1 s with no upper- and lower-stage geometries involved (plume-only configuration). Finally, a steady-state flow was calculated for stage-separation distances of 7 and 42 m that correspond to the preceding two time moments in the moving-stage configuration. To simplify analysis, the lower stage was moved relative to the upper stage, and the coordinates of the upper stage were fixed in all simulations.

The results for the four cases are given in Fig. 2, in which the translational temperature fields calculated over all gas species are presented that correspond to a time moment of 0.3 s after ignition. Only the upper half of the symmetric flow is shown, and the plume axis and both stage centerlines are aligned along the horizontal X axis. The leading edge of the upper stage is at $X = 0$ and that of the lower stage is at $X \approx 10$ m, so that the separation between them is about 7 m. The radius of the two stages is 0.345 m and so may not be visible on the scale of the figure. The temperature flowfields show two shock regions: the plume–atmosphere mixing layer in a wide swath starting at the upper-stage nozzle exit and the plume lower-stage interaction region starting at the leading-edge cap of the lower stage. The freestream velocity (5 km/s) is about two times larger than the typical plume exhaust velocity (2.5 km/s), which helps explain the higher temperature in the first region than in the flow near and after the lower stage. The maximum temperatures in these two regions are about 7200 and 2300 K, respectively. The plume–atmosphere shock mixing layers are very similar in all four cases. However, the mixing layer in the moving-stage case appears to be thinner than in the steady-state case, primarily due to the small sampling size and not the actual stage-separation process. Strictly speaking, the definition of temperature as the mathematical expectation of thermal velocity squared, $T \propto (1/N)\Sigma(u - \bar{u})^2$, assumes a large enough sample size; for a small sample size, a factor $1/(N-1)$, instead of the used $1/N$, may be a better approximation. It is also interesting to note that there are vortexlike structures formed in the mixing layer, clearly seen in Fig. 2 (top).

Statistical reasons are also behind a small difference in temperature in the lower-stage wake flow, in which the temperature is lowest for the moving stage and highest for the steady-state case. The average number of particles in a sampling cell in the wake flow region was on the order of or less than ten, which explains the inaccuracy of the temperature prediction. The five-times-longer sampling time in the fixed-body case results in higher temperatures in the wake than in the moving stage (in the latter case, the temperature calculation was meaningless for a number of cells in which less than two molecules were available for sampling). Because the wake flow is unimportant both in terms of the stage-separation and radiation predictions, further improvement of accuracy of the wake flow modeling was not pursued. Note that the longer sampling, to a large extent, smears out the vortex structures in the mixing layer that are observed in the fully transient case.

A significant conclusion from these results is the small impact of flow transience and stage motion on the gas flow in the plume–atmosphere mixing layer. Aside from statistical scatter that is visible in the three transient solutions, there is practically no difference in the location and properties of the mixing layer among the four cases. Note that the moving-stage result has larger statistical scatter than the plume-only and fixed-body cases, because the macroparameters were sampled over 0.1-ms time in the former case and 0.5 ms in the latter cases. The time to reach steady state for the first 50 m of the mixing layer is on the order of 0.01 s, which explains the similarity of the results. A smaller freestream velocity would increase the time to reach steady state, but still this would be insignificant compared with the timescale of 0.3 s.

Consider now the impact of the stage motion on the plume species density distributions. The number density fields of H_2O at 0.3 s after plume ignition are shown in Fig. 3. There is some interaction of the plume–atmosphere mixing layer and the weak shock generated by the plume-stage impingement interaction that results in a small increase in the number density at about 50 m from the nozzle. This increase is not clearly visible in the moving-stage case, in which the DSMC statistical noise is too high for subtle details of the flow to be discernible. Generally, the structure of the plume–atmosphere and plume-stage impingement shocks and the near field of the plume is quantitatively similar in the transient and steady-state cases. There are some vortexlike structures in the mixing layer noticeable in both carbon monoxide and water transient solutions, but the nature and details of these structures are out of the scope of this work.

Because of accelerations on the lower stage, the lower-stage relative velocity increases significantly with time. Starting from 2 m/s, the velocity increases to about 25 m/s at 0.3 s and then to about 75 m/s at 1 s. This relatively high velocity is still not sufficient to affect the gas properties during stage separation. This is illustrated in Fig. 4, in which the translational temperature fields are given for the moving-stage and steady-state cases at 1 s. The other two cases considered are not shown here because they are similar to the ones shown. The structure of the freestream–plume interaction region is very similar for the transient and steady-state cases and strongly resembles that of the early time moment of 0.33 s. The results indicate that the steady-state result captures all the main features of

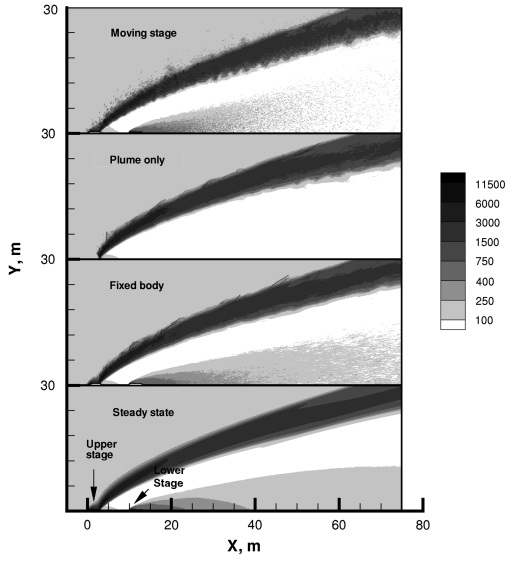

Fig. 2 Liquid propellant thruster: translational temperature (K) at 0.3 s after thruster ignition. Here and in the following figures, the direction of the freestream velocity is from left to right, going from $-x$ to $+x$.

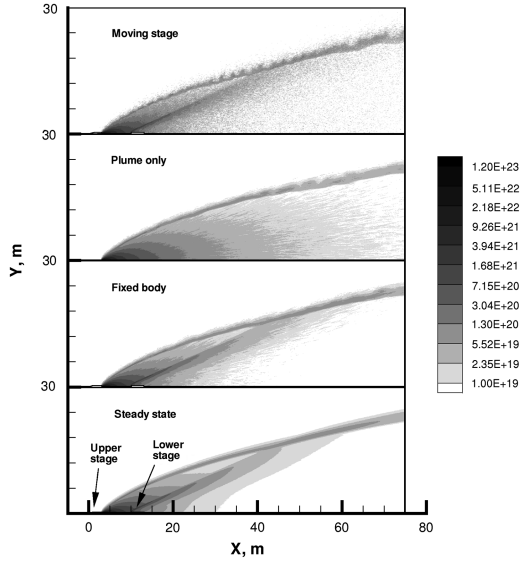

Fig. 3 Liquid propellant thruster: plume H_2O number density fields (mol/m^3) at 0.3 s after thruster ignition.

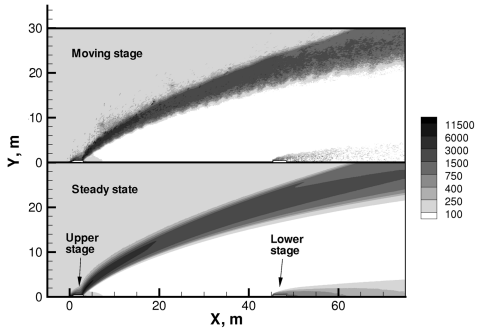

Fig. 4 Liquid propellant thruster: translational temperature fields (K) at 1.0 s after thruster ignition.

the transient result, whereas the transient case fails to adequately represent the flow near the lower stage, due to poor statistics. The total number of particles of 5 million used in the computations and the average number of particles per sampling cell of about one is obviously too small for a quality temperature evaluation. For the transient case, it is clear that a three-dimensional modeling would greatly amplify this problem, making accurate temperature estimation near the lower stage at higher separation distances prohibitively expensive from the computational standpoint at longer times.

The statistical fluctuations are even more severe when vibrational temperature is considered. Accurate prediction of vibrational temperatures is crucial for analysis of infrared (IR) signatures. The computations conducted for a discrete model of the molecular internal degrees of freedom in which we include many levels (not shown here) indicate that the vibrational temperature fluctuations may be too strong for any meaningful analysis to be conducted. For the continuous-internal-energy model, the actual impact of statistical scatter is smaller but still very strong, as illustrated in Fig. 5 for the water vibrational temperature. The temperature was averaged over 0.05 ms in the transient case to reduce the statistical noise. Still, the mixing layer and the lower-stage region temperatures are noticeably smaller than in the steady-state solution. The impact of transience on radiation signatures may not be that significant, because the maximum difference is observed in regions with very low densities of H_2O.

As a step toward a complete treatment of the radiation environment, we performed calculations with the U.S. Air Force chemistry, radiation, and signature code SOCRATES-P [11]. In Fig. 6, we show broadside infrared images of radiance from vibrationally excited gases that could be viewed from a distant sensor computed with SOCRATES-P. The calculation was performed with the same parameters as the steady-state SMILE calculation, but using a smaller simulation volume in quarter-symmetry, using 1.2 million cells in a regionally adapted grid populated by 13 million molecules. The vibrational excitations are described with two-state (ground and vibrationally excited) models, in which collisional excitation, radiation, and quenching are included. In either band, the dominant intensity source is the core flow exiting the upper-stage engine, but the H_2O radiance shows the shock structure more clearly. The slight

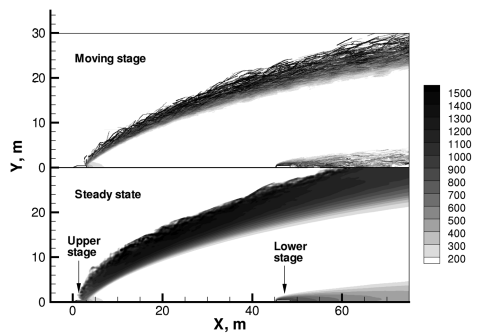

Fig. 5 Liquid propellant thruster: H_2O vibrational temperature field (K) at 1.0 s after thruster ignition.

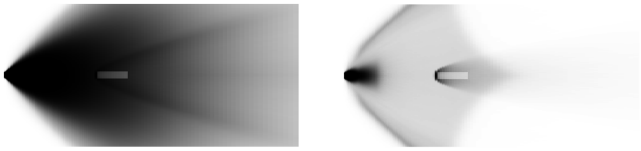

Fig. 6 Infrared images of the liquid propellant staging, as computed with SOCRATES-P for 4.7-μm excited CO (left) and 6.3-μm excited H_2O (right). The width of each image is 30 m. The intensity scale was distorted from linear using an image-processing $\gamma = 0.01$ transfer function to show the radiance enhancement near the lower stage.

chevron pattern in the water radiance imagery is an artifact of the plume–atmosphere shock leaving the solution domain, as viewed broadside. These SOCRATES-P calculations are the first step in examining the radiation environment and signature for staging scenarios.

In addition to the radiation environment, we expect that the full unsteady and quasi-steady forces will be similar. The computations have shown that the lower-stage trajectory is mostly governed by the thrust force $\mathbf{T}$, with a smaller contribution of the plume force $\mathbf{F}_p$. The distance between the upper and lower stages as a function of time is plotted in Fig. 7 for the actual stage separation observed in the computations and a separation calculated using only the initial stage velocity and thrust force propelling the upper stage (no plume force). The ignition starts at 0.02 s, and at 1 s, the distance between the stages is by about 15% larger when the plume force is included. The plume force has the biggest impact on the stage velocity during the first 0.1 s, when the separation distance is still small and the plume force impingement to lower-stage mass ratio is comparable with the thrust-to-upper-stage mass ratio. Note that even immediately after firing, the plume force on the lower stage is only about 20% of the total thrust force, both due to the plume divergence after the nozzle exit and force decrease in the shock front. Comparison of the transient force on the lower stage with the corresponding steady-state results, also given in Fig. 7, shows that there is no quantitative impact of the stage motion on the force.

An important conclusion from the modeling results of a 25-kN liquid-propellant-thruster stage separation is that the impact of the stage motion and unsteady effects on flow properties, both close and far from the moving stage, is small. This indicates that quasi-steady-state treatments for such scenarios may be quite adequate. Moreover, potential benefits of accurate prediction of the stage trajectory with transient DSMC modeling may be hindered by difficulties of flowfield and signature predictions associated with DSMC statistical scatter in transient flow modeling with the DSMC method. We also find that the impact of the plume force on the stage separation is noticeable and generally cannot be neglected.

VI. Impact of Statistical Scatter on Stage Trajectory

The application of the DSMC method to modeling stage separation may imply a significant level of statistical scatter in the

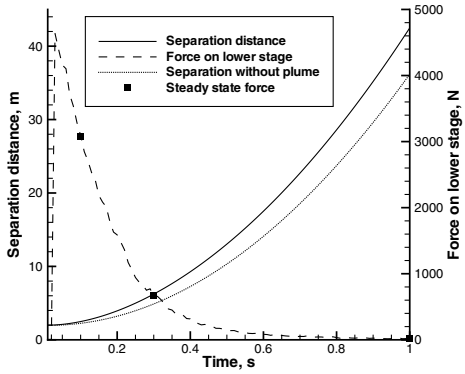

Fig. 7 Liquid propellant thruster: temporal profiles of the separation distance (solid line), force on the lower stage (long dashed line), and separation without plume (dotted line).

computation of the force from the plume impingement on the lower stage. In the computations presented in the previous section, the plume force was estimated based on no more than a few thousand gas–surface collisions, even for smaller separation distances. For larger distances, the number of surface collisions decreases by almost three orders of magnitude, although the impact of the plume force compared with the thrust force also decreases drastically. Generally, a strong dependence of the stage trajectory on the accuracy of the force calculation signals that the number of particles used is not adequate and needs to be increased or a spatial weighting approach to increase this accuracy may have to be developed and applied.

To analyze the possible contribution of statistical scatter to the stage trajectory predictions, DSMC computations were performed for different numbers of simulated particles. This set of computations was performed using the same nozzle exit flow properties as for the preceding axisymmetric computations, but in a two-dimensional Cartesian treatment. A 2D Cartesian consideration allows one to include body rotation as well as deviation from the plume axis, which is not possible in an axisymmetric modeling. Note that the use of the same number density and flow velocity at the nozzle exit results in an effectively much higher thrust at the lower stage in 2D, thus amplifying the effect of the plume.

The computations are conducted for three values of the total number of simulated molecules, 5, 1, and 0.2 million. Analysis of the results has shown that gas flowfield solutions are qualitatively similar for these three cases, whereas a quantitative comparison is complicated by significant statistical scatter when lower numbers of particles are used. The influence of the scatter in the plume force evaluation on the total separation distance measured as the closest distance between the two stages is given in Fig. 8 (left). Although there is a visible difference between the separation distance for different numbers of particles, these differences are much smaller than their difference in the case when the stage moved only due to the thrust propelling the upper stage.

In an ideal case of a fully symmetric plume, there should be no deviation of the stage center of mass from the plume axis. The moving lower stage should always be aligned with this axis because the lift force and the pitching moment are zero. However, the statistical noise inherent in any DSMC modeling results in the lift and torque forces on the moving stage. Moreover, the stage translation off the axis and the rotation further increase these forces due to created asymmetry. The effect of the statistical scatter on the distance between the lower-stage center of mass and the plume axis is given in Fig. 8 (center). The conclusion here is that the impact of the number of particles on the stage deviation from the axis is negligible. This is because the lift force is small compared with the drag force, and the positive and negative values of the lift force at consecutive displacements of the lower stage nearly equilibrate over time.

Similarly, the rotation of the stage is insignificant during the first second after stage ignition, as illustrated in Fig. 8 (right). It is also important to mention that the results of this section are for 2D Cartesian geometries, and the impact of the plume force is strongly amplified by a factor of 5, compared with the corresponding axisymmetric (and 3D) case. Such a weak dependence of the lower-stage trajectory on statistical fluctuations caused by a limited number of gas–surface collisions is an indication that even a full 3D DSMC modeling is possible for a moving lower stage with an acceptable accuracy of trajectory estimation.

VII. Solid Propellant Thrusters

The weak dependence of the stage-separation modeling results on the stage motion and unsteady nature of the flow is primarily related to the relatively fast time to reach steady state both in the plume stage and in the plume–freestream interaction regions. Usually, the flow needs a longer time to reach steady state for solid propellant rocket thrusters, because the plume is two-phase and includes both gas and alumina particle transport. The particulates typically move slower than gas, and there is also some gas–particle interaction, which both result in a longer transient time than for liquid propellant thrusters under similar conditions. To study the effect of particulates on the transient stage separation, the DSMC computations were conducted for a 35-kN solid propellant thruster with stagnation gas parameters similar to the previously considered liquid propellant case and for two sizes of particulates, small and large, with diameters of 0.2 and 3.6 μm, respectively. As previously mentioned, a close-to-maximum particle loading of 20% was used to emphasize the effect of particles.

The gas and particle properties at the nozzle exit plane obtained with the CFD++ continuum solver are shown in Fig. 9. As the gas density profile clearly shows, there is a noticeable boundary layer formed at the nozzle surface. The density of the small particulates is qualitatively very similar to the gas density, because the mass of these particles is too small to be different from the gas (the gas and 0.2-μm particle velocities practically coincide). The drag force on larger alumina particles is not high enough for them to move along gas streamlines, and their number density shape differs from that of the gas. Note that only the large-particle surface temperature is presented in Fig. 9, because the surface temperature of smaller particles coincides with that of the gas. It is important to note that both the small- and large-particle temperatures are noticeably lower than the alumina melting temperature of 2325 K, which means that the particles have already solidified while traveling in the diverging part of the nozzle. Note that an equilibrium particle crystallization model was used in the continuum simulations, which generally implies an immediate transition of particles that reached the melting temperature from a liquid to a solid state. The actual crystallization process is nonequilibrium, with gradual particle solidification that starts at some critical temperature below the melting temperature; this may affect particle temperatures in the plume to some extent.

We now consider the effect of the stage motion and unsteady effects on gas and particulate properties. The gas-temperature fields for a stage separation at 0.3 s after the thruster ignition are shown in Fig. 10. The distance between the stages at this time moment is about 7 m. In Figs. 10 and 11, the top half illustrates the results of the transient flow development with the moving lower stage, and the

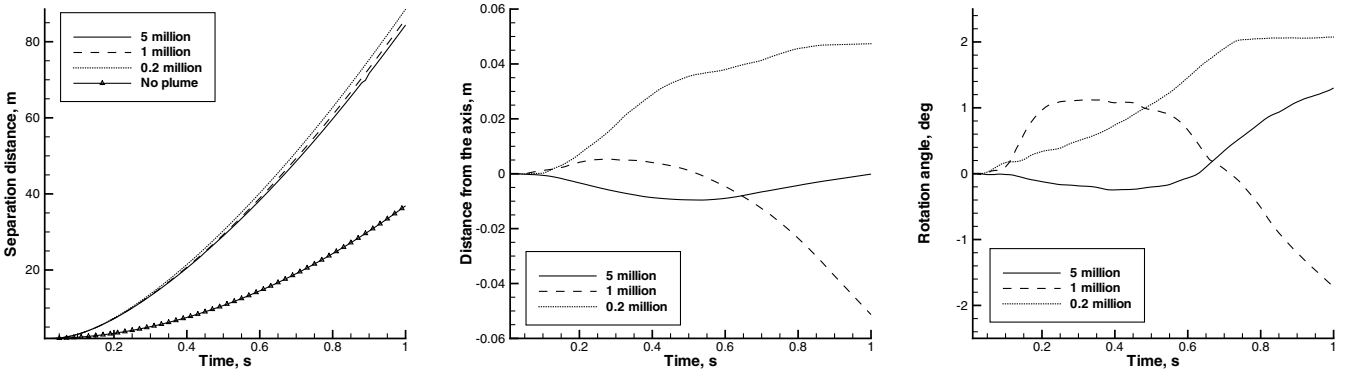

Fig. 8 Two-dimensional Cartesian liquid propellant case: the impact of the number of simulated particles on stage-separation distance (left), deviation from the plume axis (center), and the rotation angle (right); 5 million (solid line), 1 million (long dashed line), and 0.2 million (dotted line).

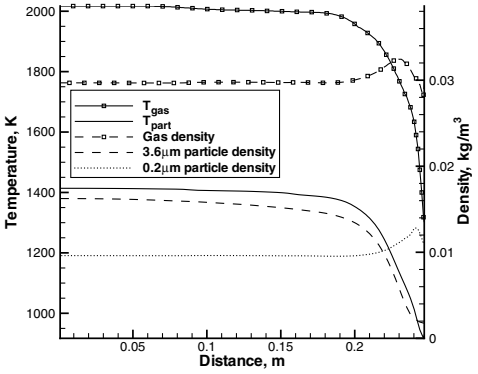

Fig. 9 Solid propellant thruster: flow properties across the nozzle exit plane.

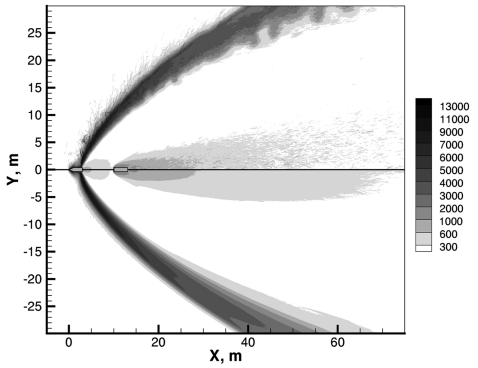

Fig. 10 Solid propellant thruster: gas translational temperature (K) at 0.3 s after thruster ignition. The top half shows the unsteady results and the bottom half shows the steady-state results.

lower half shows the results of the steady-state modeling with the distance between the stages that corresponds to the transient case. Comparison of the results shows that there is no significant impact of the flow transience, similar to the liquid case considered. The gas temperature in the wake is somewhat lower in the transient case, which is attributed to the relatively small number of particles in this rarefied region and not to the actual motion of the stage. As was previously mentioned, $T \propto [1/(N-1)]\Sigma(u-\bar{u})^2$ may be a better approximation than the standard definition of temperature as mathematical expectation of thermal velocity squared.

Comparison of the transient and steady-state number density fields of large particles at 0.3 s is given in Fig. 11. It is clear that there is generally a very good agreement between the two solutions. Note that the results for smaller particles agree as well. For both particle sizes, there is an increase in the number density in the shock front near the lower stage. Smaller particles follow the gas streamlines in

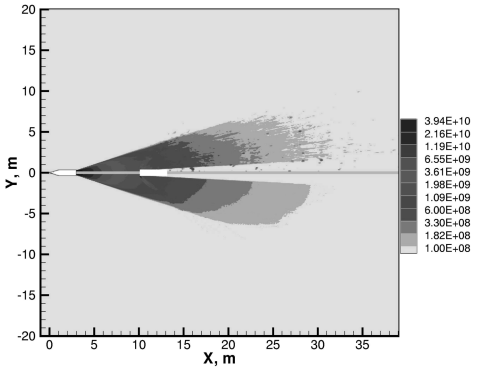

Fig. 11 Solid propellant: number density fields (molecule/m^3) of large particulates at 0.3 s after separation. The top half shows the unsteady results and the lower half shows the steady-state results.

the bow shock and then in the expansion region. Because of their large mass, the 3.6-μm particles reflected from the body are impacted by the gas to a lesser extent than the smaller particles and do not follow gas streamlines in the bow shock. The trajectories of the large particles that did not collide with the stage are weakly changed by the bow shock. Note also that the particle temperatures do not change significantly throughout the computational domain outside the shock region in front of the lower stage. In that small region, the smaller particle temperature first increases above the melt temperature and then drops below the melt temperature near the surface. This indicates that the smaller particles are likely to melt and be in the liquid states during their collisions with the body. The particle melting was not modeled in this work. The temperature of the larger particles reaches a maximum of about 2280 K inside the shock. Generally, special care needs to be taken when modeling the interaction of particles traveling through the shock with the stage surface, but the details of this process were not in the scope of this work. The important conclusion here is that the gas and particle behavior is not visibly impacted by the stage motion.

VIII. Conclusions

The direct simulation Monte Carlo method was used to simulate the staging process of a generic sounding rocket at an altitude of 100 km. Both liquid and solid propellants were modeled, with thrust levels of 25 and 34 kN, respectively. A CFD++ commercial Navier–Stokes solver was used to predict the gas and particulate properties at the nozzle exit plane. The 2D Cartesian/axisymmetric module of the DSMC-based solver SMILE was then used to calculate the flow from the exit plane. For these calculations, SMILE was extended to include the body motion, and all unsteady flow effects were included. Both constant thrust force and time-dependent plume force on the lower stage were considered. The acceleration of the lower stage relative to the upper stage varied from about 14 g immediately after the ignition to about 7 g at 1 s after ignition.

From our DSMC stage-separation results, we have seen that the engine startup produces a plume that establishes a shock with the atmosphere. The plume's impingement on the lower stage creates a second shock and a stagnation region near the plume impact on the lower stage. This second shock is established quickly, and it persists but becomes weaker as the stages move away from each other. Although the two shock structures may intersect weakly downstream (see Fig. 3 at 40 m downstream of the nozzle exit), there is almost no interaction between the two shock structures. To analyze the impact of the lower-stage motion, in addition to the fully transient case, computations were performed for a transient plume with a fixed body within a steady-state treatment (i.e. quasi-steady assumptions), with the stage-separation distance corresponding to that of the fully transient case. The computations showed that the stage motion and other unsteady flow effects have little influence on the results of the computations, compared with the steady-state cases. This result is consistent with the much faster timescale of the molecular gas–gas collisions than the timescale for motion of the solid body. This indicates that quasi-steady-state modeling may be preferred for these scenarios, due to inherently better convergence. There are some small differences between the steady and unsteady solutions in flow regions with relatively small numbers of simulated particles. These differences are attributed to the poorer statistics of the transient solutions compared with the steady-state solutions. These conclusions hold both for liquid and solid propellant rockets and may be generalized to staging processes with lower-stage accelerations.

It is important to establish the need to explicitly include time dependence in such fluid flow calculations, because it can incur a large computational expense. One approximate way to do this before undertaking potentially time-consuming computations is to examine the basic timescales of motion. A fundamental timescale for gas–gas collisions is the local molecular collision time t. If the solid body can move a substantial distance within a molecular collision period, the motion of the body will be coupled to the gas flow. A way to quantify the relative timescales of the molecular collision period and the

solid-body motion is the ratio of the mean free path λ divided by the collision time t to the speed of the solid body v_{solid}: $\lambda/(t \cdot v_{\text{solid}})$. When this ratio is much greater than one, the gas–gas collision times are much less than the solid-body motion time. In this case, a quasi-steady-state treatment, in which the solid-body motion is "frozen" along its trajectory and several independent steady-state calculations are done, should be sufficient. For the present scenarios with the number density on the order of 5×10^{20} m^{-3}, a mean molecular speed $\sim$1500 m/s, and using a molecular cross section of 10^{-19} m^2, we find a ratio of $\sim 60 \gg 1$. This confirms that a quasi-steady-state treatment should be nearly equivalent to a fully coupled time-dependent treatment of the body motion, as we observe. Of course, this simplified approach is approximate because it does not take into consideration the actual scales of the flow development that generally should be accounted for.

The impact of the statistical fluctuations on the stage-separation trajectory was studied for a 2D Cartesian flow and was found relatively small compared with the general impact of the plume force on the stage-separation distance. This conclusion is applicable to separation distance, motion in the transverse direction, and rotation. These findings are explained by the fact that the motion due to the lift force and pitching moment is small compared with that caused by the drag force. The positive and negative values of the lift force and pitching moment at consecutive displacements of the lower stage due to statistical scatter nearly equilibrate over time. These results may also be an indication that similar transient scenarios can be examined in full 3D with little concern over DSMC statistical errors from surface force fluctuations.

As a step toward a complete treatment of the staging radiation environment, we also performed calculations with the U.S. Air Force chemistry, radiation, and signature code SOCRATES-P [11]. IR radiance imagery generated from these preliminary calculations reveals the plume–atmosphere shock structure and plume–lower-stage impingement radiation. These SOCRATES-P calculations are the first step in examining the full transient radiation environment and signature for staging scenarios.

Acknowledgments

The authors gratefully acknowledge partial support of this work from a Missile Defense Agency (MDA) Small Business Innovative Research (SBIR) award under contract W9113M-06-C-0122. Sergey Gimelshein is thankful to Dean Wadsworth for fruitful discussions.

References

[1] Bird, G.A., *Molecular Gas Dynamics and the Direct Simulation of Gas Flows*, Clarendon Press, Oxford, 1994.

[2] Oran, E. S., Oh, C. K., and Cybyk, B. Z., "Direct Simulation Monte Carlo: Recent Advances and Applications," *Annual Review of Fluid Mechanics*, Vol. 30, 1998, pp. 403–441. doi:10.1146/annurev.fluid.30.1.403

[3] Gallis, M. A., and Torczinki, J. R., "Simulation of Moving Microbeams with the Direct Simulation Monte Carlo Method," AIAA Paper 2003-4013, 2003.

[4] Cavallo, P. A., Sinha, N., and Feldman, G. M., "Parallel Unstructured Mesh Adaptation for Transient Moving Body and Aeropropulsive Applications," AIAA Paper 2004-1057, 2004.

[5] Ivanov, M. S., Markelov, G. N., and Gimelshein, S. F., "Statistical Simulation of Reactive Rarefied Flows: Numerical Approach and Applications," AIAA Paper 98-2669, 1998.

[6] Ivanov, M. S, and Rogasinsky, S. V., "Analysis of Numerical Techniques of the Direct Simulation Monte Carlo Method in the Rarefied Gas Dynamics," *Soviet Journal of Numerical Analysis and Mathematical Modelling*, Vol. 2 No. 6, 1988, pp. 453–465.

[7] *CFD++ User Manual, Version 5.1.1*, Metacomp Technologies, Agoura Hills, CA, 2005.

[8] Merkle, C. L., Behrens, H. W., and Hughes, R. D., "Application of the Monte-Carlo Simulation Procedure in the Near Continuum Regime," *Rarefied Gas Dynamics*, edited by S. S. Fisher, Progess in Astronautics and Aeronautics, Vol. 74, AIAA, New York, 1981, pp. 256–268.

[9] Gallis, M. A., Torczynski, J. R., and Rader, D. J., "An Approach for Simulating the Transport of Spherical Particles in a Rarefied Gas Flow Via the Direct Simulation Monte Carlo Method," *Physics of Fluids*, Vol. 13, No. 11, 2001, pp. 3482–3492.

[10] Gimelshein S., Alexeenko A., Wadsworth D., and Gimelshein N., "The Influence of Particulates on Thruster Plume/Shock Layer Interaction at High Altitudes," AIAA Paper 2005-766, 2005.

[11] Braunstein M., and Cline, J. A., "Progress on Parallelizing a General Purpose Direct Simulation Monte Carlo (DSMC) Code for High Performance Computing Applications" NASA Marshall Space Flight Center, Publication 20030107284, Huntsville, AL, 2003.

I. Boyd
Associate Editor